

AGN jet power and feedback characterised by Bondi accretion in brightest cluster galaxies

Yutaka Fujita^{1*}, Nozomu Kawakatu², and Isaac Shlosman^{3,1}

¹*Department of Earth and Space Science, Graduate School of Science, Osaka University, 1-1 Machikaneyama-cho, Toyonaka, Osaka 560-0043, Japan*

²*Faculty of Natural Sciences, National Institute of Technology, Kure College, 2-2-11 Agaminami, Kure, Hiroshima, 737-8506, Japan*

³*Department of Physics and Astronomy, University of Kentucky, Lexington, KY 40506-0055, USA*

Accepted 0000 December 00. Received 0000 December 00; in original form 0000 October 00

ABSTRACT

We propose a new method to estimate the Bondi (hot gas) accretion rates, \dot{M}_B , onto the supermassive black holes (SMBHs) at the centres of elliptical galaxies. It can be applied even if the Bondi radius is not well-resolved in X-ray observations and it is difficult to measure the gas density and temperature there. This method is based on two simple assumptions: (1) hot gas outside the Bondi radius is in nearly a hydrostatic equilibrium, and (2) the gas temperature near the galaxy centre is close to the virial temperature. We apply this method to 28 bright elliptical galaxies in nearby galaxy clusters (27 of them are the brightest cluster galaxies; BCGs). We find a correlation between the Bondi accretion rates and the power of jets associated with the SMBHs over four orders of magnitude in \dot{M}_B . For most galaxies, the accretion rates are large enough to account for the jet powers, which is in contrast with previous studies. Our results indicate that the feedback from the active galactic nuclei (AGN) correlates with the properties of the hot gas surrounding the SMBHs. We also find that more massive SMBHs in BCGs tend to have larger specific growth rates. This may explain the hyper masses ($\sim 10^{10} M_\odot$) of some of the SMBHs. Comparison between the accretion rates and the X-ray luminosities of the AGN suggests that the AGN in the BCGs are extremely radiatively inefficient compared with X-ray binaries in the Milky Way, even when their Eddington accretion ratio, $\dot{M}_B/\dot{M}_{\text{Edd}}$, exceeds 0.01. The corollary is that this ratio is not the only parameter which controls the radiative efficiency of the accretion flow. Lastly, we find a tight correlation between the Bondi accretion rates and the X-ray luminosities of cool cores. Their relation is linear and the power generated by the Bondi accretion is large enough to compensate the radiative cooling of the cool cores. Although the ‘classical’ Bondi accretion model is a greatly oversimplified one, the correlations we find here demonstrate that the accretion onto the SMBHs reflects broadly the properties of the Bondi accretion in some time-averaged sense.

Key words: accretion, accretion discs — black hole physics — galaxies: active — galaxies: jets — X-rays: galaxies.

1 INTRODUCTION

Energetic feedback from active galactic nuclei (AGN) is thought to prevent the cooling of hot gas in galaxies and clusters of galaxies, delaying or suppressing star formation in these objects (Bower et al. 2006; Best et al. 2006). However, the mechanism that controls the level of activity is not well known. The AGN located at the centres of the brightest cluster galaxies (BCGs) can play an important role in preventing the development of “cool-

ing flows”, which would have developed in the absence of the AGN feedback (McNamara & Nulsen 2007). However, AGN feedback in cool cores of clusters is often subject to a global thermal instability (e.g. Fujita & Suzuki 2005; Mathews, Faltenbacher, & Brighenti 2006). Even if the thermal instability does not develop with the aid of thermal conduction or cosmic rays (Ruszkowski & Begelman 2002; Guo & Oh 2008; Fujita, Kimura, & Ohira 2013), the AGN must respond quickly, on a dynamical or a sound crossing timescale in the core, to the change of the environment (e.g. gas density and temperature) to maintain the balance between the heating and the radiative cooling.

* E-mail: fujita@vega.ess.sci.osaka-u.ac.jp

The Bondi accretion (Bondi 1952) is a promising route for the gas supply to the central supermassive black holes (SMBHs) in the BCGs. Since accretion rate depends on the density and temperature of the surrounding hot gas (see equation 1), the AGN activity can respond accordingly to the change of the state of this gas. The AGN feedback to the Bondi accretion has been detected by studying 9 nearby, X-ray luminous elliptical galaxies (not all of them being BCGs) with *Chandra X-Ray Observatory* (Allen et al. 2006); a correlation between the Bondi accretion rates (inferred from the observed gas temperature and density profiles, and SMBH masses) and the AGN power (in the form of relativistic jets) has been shown to exist. Successive studies have confirmed this correlation (Balmaverde, Baldi, & Capetti 2008; Vattakunnel et al. 2010), although observational uncertainties exist (Russell et al. 2013).

For BCGs in general, the correlation has not been firmly established, partly because observational uncertainties appear to be substantial due to the large average distance to the BCGs. Moreover, apparent jet powers seem to be insufficient to compensate for the radiative cooling of cool cores of some clusters (Bîrzan et al. 2004; Rafferty et al. 2006). As an alternative to the Bondi hot gas accretion, cold gas accretion may work. In fact, cold gas has been detected in many elliptical galaxies including BCGs (e.g. Edge 2001; Werner et al. 2014), and some of them even have cold gas discs (Fujita et al. 2013; Hamer et al. 2014), which could power the jets. While the cold gas accretion is generally more efficient in producing the AGN radiation, the associated accretion processes could involve complicated physics, such as dynamical instabilities and disc cooling. Thus, it is not certain whether the AGN can respond sufficiently quickly and accordingly to the changes in the environment. Finally, no correlation between AGN jet power and total molecular gas mass is known to exist (McNamara, Rohanizadegan, & Nulsen 2011), which suggests that simple accretion of the molecular gas does not control the AGN activities in BCGs at low redshifts.

In this paper, we investigate whether accretion onto the SMBHs in BCGs can be characterised by the Bondi accretion in the broad sense, by studying the correlation between the accretion rate and the AGN jet power. We also compare the power available through the Bondi accretion with the X-ray AGN and cool core luminosities to study the radiation efficiency of the accretion discs and suppression of the cooling flows. For these studies, we devise a new method to estimate the Bondi accretion rate. The rest of the paper is organised as follows. In Section 2, we describe the details of our method to calculate the Bondi accretion rate. The data used in the analysis are presented in Section 3, and the results are provided in Section 4. Section 5 is devoted to discussion of the SMBH accretion and the heating of cluster cool cores. Our main conclusions have been summarised in Section 6. We assume cosmological parameters of $\Omega_{m0} = 0.3$, $\Omega_{\Lambda 0} = 0.7$, and $h = 0.7$, which are often used in this field. Unless otherwise noted, errors are the 1σ values.

2 METHOD

We assume that hot gas accretion onto the SMBHs at the centres of our sample galaxies is not dominated by the an-

gular momentum and, therefore, take it to be spherically-symmetric. The Bondi accretion rate is given by

$$\dot{M}_B = 4\pi\lambda_c(GM_\bullet)^2 c_{s,B}^{-3} \rho_B = \pi\lambda_c c_{s,B} \rho_B T_B^2, \quad (1)$$

where M_\bullet is the SMBH mass, and $\rho_B = \rho(r_B)$ and $c_{s,B} = c_s(r_B)$ are the density and the sound speed at the Bondi accretion radius $r_B = 2GM_\bullet/c_{s,B}^2$ (Bondi 1952). The coefficient λ_c depends on the adiabatic index of the accreting gas (γ) and we assume $\gamma = 5/3$ and $\lambda_c = 0.25$. The sound speed $c_s = \sqrt{\gamma k_B T / (\mu m_p)}$ is the function of gas temperature T , where $\mu (= 0.6)$ is the mean molecular weight, and m_p is the proton mass. Equation (1) shows that the information on M_\bullet , ρ_B , and $T_B (= T(r_B))$ are required to evaluate \dot{M}_B . Even with the superb angular resolution of *Chandra*, an expected Bondi radius of any system in our sample cannot be resolved. Thus, we need to extrapolate the density and temperature at the innermost measurement radius (r_{obs}) to those at the Bondi radius. In previous studies, the extrapolation was made by assuming a power-law for the density profiles and a constant temperature (Allen et al. 2006; Balmaverde, Baldi, & Capetti 2008). However, it is not certain whether such an assumption is physically justified. Moreover, since the distances to the BCGs are generally large, this method could cause large errors. Thus, a more physical method for the extrapolation is required.

For this extrapolation, we made two assumptions. First, we assume that the hot gas outside the Bondi radius is in a nearly hydrostatic equilibrium:

$$-\frac{dP}{dr} = \rho g, \quad (2)$$

where $P(r)$ is the thermal gas pressure, and $g(r)$ is the gravitational acceleration. For some nearby clusters (e.g. Perseus; Fabian et al. 2006), it has been revealed that the innermost region is strongly disturbed by AGN activities. However, the assumption of the hydrostatic equilibrium can be still acceptable as long as the turbulent and ram pressures associated with the gas motions are smaller than its thermal pressure. While the actual gas velocity has not been measured, it will be obtained with *Astro-H* in the near future. The second assumption is that the gas temperature near the SMBH (i.e., at $r \sim r_B$) reflects the velocity dispersion σ or the virial temperature $T_{\text{gal,vir}}$ of the host galaxy:

$$T_0 = \beta^{-1} \frac{\mu m_p \sigma^2}{k} \sim T_{\text{gal,vir}}, \quad (3)$$

where k is the Boltzmann constant, and β is the constant of order of unity. Following Matsushita (2001), we adopt $\beta = 0.5$ for massive elliptical galaxies including BCGs. The second assumption is related to the first one, because the left-hand side of equation (2) is approximated by $-dP/dr \sim P/r = nkT/r$, where n is the number density of the gas, while the right-hand side is approximated by

$$\rho g = \rho \frac{GM(<r)}{r^2} \sim n \frac{kT_{\text{gal,vir}}}{r}, \quad (4)$$

where $M(<r)$ is the gravitational mass within the radius r . The second assumption, i.e., equation (3), is generally consistent with *ROSAT* X-ray observations (Matsushita 2001). In Section 4, we discuss the temperature profiles in the central regions of nearby BCGs obtained with recent *Chandra* observations.

We assume that the temperature profile reflects the size of the galaxy and the profile between $r = r_B$ and r_{obs} is given by

$$T(r) = T_0 + (T_{\text{obs}} - T_0) \frac{\tanh(r/R_e)}{\tanh(r_{\text{obs}}/R_e)}, \quad (5)$$

where $T_{\text{obs}} = T(r_{\text{obs}})$ and R_e is the effective radius (half-light radius) of the galaxy. Thus, the temperature decreases toward the galaxy centre in general. Once $T(r)$ is determined, the Bondi radius r_B can be derived by numerically solving the equation

$$r_B = \frac{2GM_\bullet}{c_s(T(r_B))^2} \quad (6)$$

for a given M_\bullet .

The equation of the hydrostatic equilibrium (equation 2) can be written as

$$\frac{d\rho}{dr} = -\frac{\rho}{T} \left(\frac{\mu m_p}{k} g + \frac{dT}{dr} \right). \quad (7)$$

Since $T(r)$ has been determined by equation (5), $\rho(r)$ can be obtained by numerically integrating equation (7) and setting $\rho_{\text{obs}} = \rho(r_{\text{obs}})$ and $g(r)$. The electron number density is given by $n_e = \rho/(1.13 m_p)$.

The gravitational acceleration g is given by three components, i.e., $g = g_\bullet + g_{\text{gal}} + g_{\text{cl}}$, where g_\bullet is the SMBH contribution, g_{gal} is the galaxy contribution, and g_{cl} comes from the cluster (Mathews, Faltenbacher, & Brighenti 2006; Guo & Mathews 2014). Thus,

$$g_\bullet = \frac{GM_\bullet}{r^2}. \quad (8)$$

The acceleration from a galaxy with the Hernquist profile (Hernquist 1990) is

$$g_{\text{gal}} = \frac{GM_{\text{gal}}}{(r + r_H)^2}, \quad (9)$$

where M_{gal} is the stellar mass of the galaxy, and $r_H = R_e/1.815$. The cluster acceleration for the NFW profile (Navarro, Frenk, & White 1996) is

$$g_{\text{cl}} = \frac{GM_{\text{vir}}}{r^2} \frac{\log(1+y) - y/(1+y)}{\log(1+c_{\text{vir}}) - c_{\text{vir}}/(1+c_{\text{vir}})}, \quad (10)$$

where $y = c_{\text{vir}} r / r_{\text{vir}}$, and c_{vir} is the concentration parameter. The cluster virial radius, r_{vir} , is defined as the radius at which the average cluster density is $\Delta(z)$ times the critical density $\rho_{\text{crit}}(z)$ at the cluster redshift z :

$$r_{\text{vir}} = \left(\frac{3M_{\text{vir}}}{4\pi\Delta(z)\rho_{\text{crit}}(z)} \right)^{1/3}. \quad (11)$$

For $\Delta(z)$, we use the fitting formula of Bryan & Norman (1998): $\Delta = 18\pi^2 + 82x - 39x^2$, where $x = \Omega_m(z) - 1$.

To summarise, we require the parameters z , M_\bullet , M_{gal} , R_e , σ , c_{vir} , and M_{vir} , and the boundary conditions r_{obs} , ρ_{obs} , and T_{obs} in order to obtain r_B and \dot{M}_B . First, $T(r)$ is determined by equations (3) and (5) for given σ , T_{obs} , R_e , and r_{obs} . The Bondi radius r_B is estimated by solving equation (6) for given $T(r)$ and M_\bullet . Then, $\rho_B = \rho(r_B)$ is obtained by integrating equation (7) from $r = r_{\text{obs}}$ to r_B using equations (8)–(11) for given $T(r)$, M_\bullet , M_{gal} , R_e , M_{vir} , c_{vir} and z . The Bondi accretion rate is given by equation (1).

3 DATA

Accounting for data uniformity and consistency, we study 28 bright elliptical galaxies in clusters, for which the properties of the central gas, the excavated cavity, etc., are well studied by Rafferty et al. (2006, see their Table 6). They are BCGs except for M84. The parameters for the gravitational potentials are shown in Table 1. For the masses of the SMBHs, we adopt those derived by McNamara, Rohanizadegan, & Nulsen (2011). The masses were estimated using R -band absolute magnitudes (M_R) obtained by Rafferty et al. (2006). Since the errors in M_\bullet were not given, we take them as 0.5 dex, based on the dispersion around the observed M_R – M_\bullet relations (e.g. McLure & Dunlop 2002). The galaxy masses (M_{gal}) were estimated by Rafferty et al. (2006) using the R -band absolute magnitudes, and thus they are consistent with M_\bullet . The effective radii of the galaxies (R_e) are from the 2MASS All-Sky Extended Source Catalogue¹. We take the average of R_e in the J , H and K -bands, and their scatter as the error. The velocity dispersions of the galaxies (σ) are taken from the HyperLeda database². However, 12 galaxies have no data. For those galaxies, we use the error-weighted average of the remaining 16 galaxies (289.5 km s^{-1}) as σ , and the scatter of these galaxies, $\sim 289.5 \text{ km s}^{-1}$, as the error of σ (35.9 km s^{-1}).

The parameters for the clusters are also shown in Table 1. Most of them are based on recent X-ray observations. For the clusters with no appropriate X-ray data, we adopt the data obtained through lensing observations or kinematics of the member galaxies. For M84, HCG 62, and 3C 388, we do not consider the contribution of the cluster component to the total gravitational acceleration g , because M84 is not a BCG and there are no appropriate data for the other two. Since the errors of c_{vir} and M_{vir} were not given for MS 0735.6+7421 (Molikawa et al. 1999), they are assumed to be 0.3 dex. For Hercules A and Cygnus A, we use the cluster temperatures and the core radii obtained by Gizani & Leahy (2004) and Smith et al. (2002), respectively. The temperatures are converted into the cluster masses M_{vir} by using the cluster mass–temperature relation derived by Sun et al. (2009). The core radii (r_c) are converted into the characteristic radii ($r_s = r_{\text{vir}}/c_{\text{vir}}$) by using the relation of $r_s = r_c/0.22$ (Makino, Sasaki, & Suto 1998).

The boundary conditions r_{obs} , $n_{e,\text{obs}} (= n_e(r_{\text{obs}}))$, and T_{obs} shown in Table 2 are the same as those in Table 6 of Rafferty et al. (2006). In their table, r_{obs} , $n_{e,\text{obs}}$, and T_{obs} are represented by a , n_e , and kT , respectively. Although Rafferty et al. (2006) give the average densities and temperatures for $r < r_{\text{obs}}$ excluding the AGN, most of the emission comes from $r \sim r_{\text{obs}}$, because the density profiles near the galaxy centres are not very steep ($\alpha \lesssim 1$ for $\rho \propto r^{-\alpha}$) as is shown later. In other words, the density profiles we have obtained do not produce excessively bright emission from the gas in the vicinity of the AGN, and appear to be consistent with the observations.

¹ <http://irsa.ipac.caltech.edu/cgi-bin/Gator/nph-query>

² <http://leda.univ-lyon1.fr/>

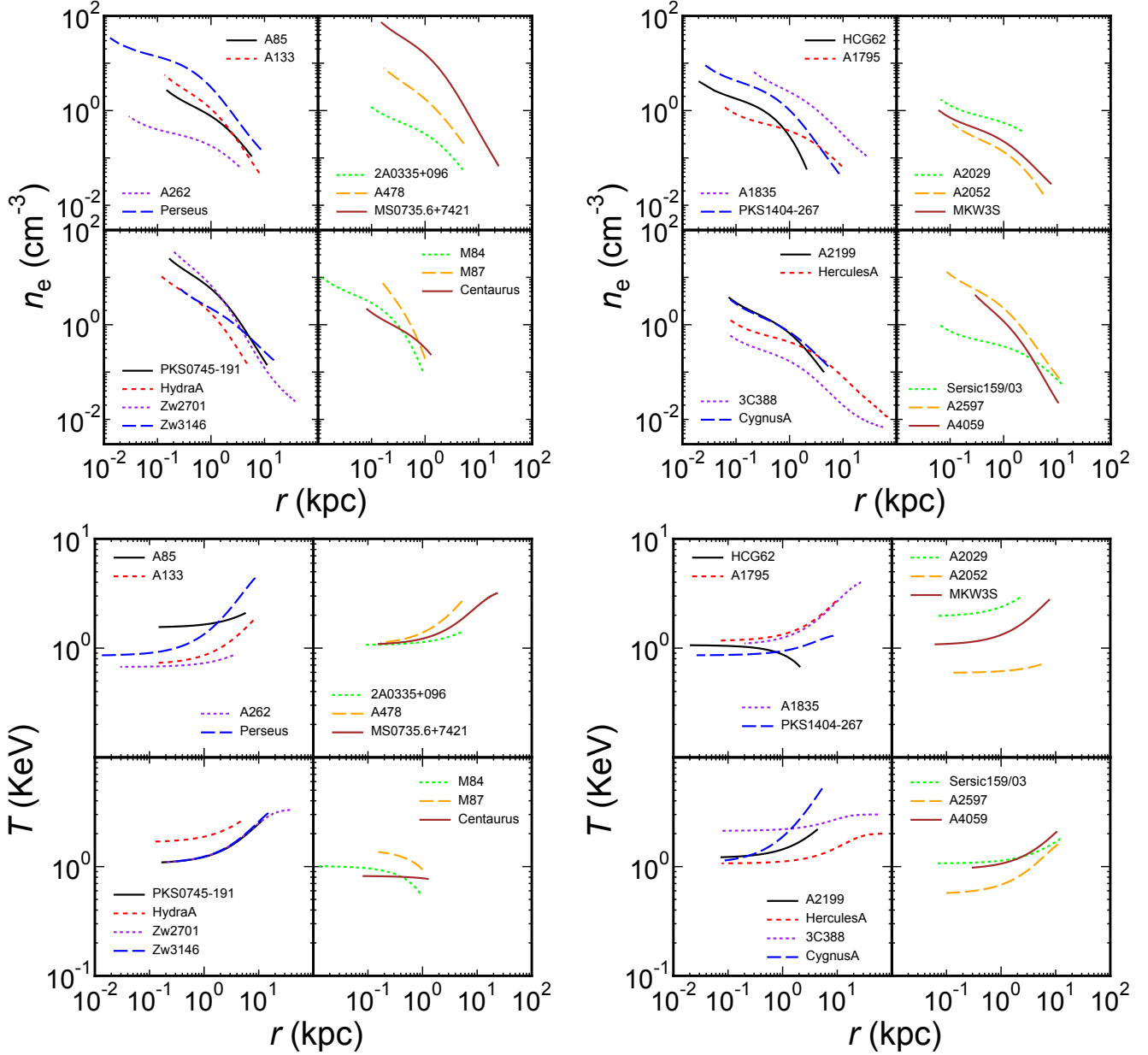


Figure 1. Most probable density and temperature profiles for our sample galaxies. The right end left ends of each curve correspond to r_{obs} and r_{B} , respectively.

4 RESULTS

In Table 3, we present the Bondi accretion radii, r_{B} , the density, $n_{\text{e,B}} = n_{\text{e}}(r_{\text{B}})$, and the temperature, $T_{\text{B}} = T(r_{\text{B}})$, at these radii. The Bondi accretion rates are also shown. The obtained Bondi radii are substantially larger than those in Rafferty et al. (2006), because we adopt smaller T_{B} . The uncertainties of the results were estimated using Monte Carlo simulations. We randomly perturbed each input parameter with a Gaussian distribution of the perturbations, which had an amplitude determined by the error bar of the parameter. We obtained 10^4 different realisations. Fig. 1 shows the density and the temperature profiles between r_{B} and r_{obs} . While the density profiles can be represented by a power-law for most clusters, some profiles show noticeable bends.

This means that a power-law is not always a good assumption when extrapolating the density profile from r_{obs} to r_{B} . For nearby galaxies such as M84, M87, and Centaurus, the gas properties near the centres are observationally known ($r_{\text{obs}} \sim 1$ kpc). For these galaxies, the temperatures at $r \sim r_{\text{obs}}$ are close to T_0 , which supports our assumption that the gas in the central region of a galaxy is close to the virial temperature of the galaxy.

The maximal power released from the neighbourhood of the SMBH through the Bondi accretion is

$$P_{\text{B}} = \eta \dot{M}_{\text{B}} c^2, \quad (12)$$

where η is the accretion efficiency assumed $\eta = 0.1$. We compare the Bond accretion power with the kinetic power of the jets, P_{jet} . We use the jet power esti-

mated as the ratio of the enthalpy of cluster X-ray cavities to their buoyancy timescales (Rafferty et al. 2006; McNamara, Rohanizadegan, & Nulsen 2011). The enthalpy is given by

$$E_{\text{cav}} = \frac{\gamma_c}{\gamma_c - 1} P_s V_c, \quad (13)$$

where P_s is the pressure of the gas surrounding the cavity, V_c is the cavity's volume, and γ_c is the adiabatic index of the gas inside the cavity. Rafferty et al. (2006) and McNamara, Rohanizadegan, & Nulsen (2011) assumed that the cavities are filled with ultra-relativistic cosmic rays, which means that $\gamma_c = 4/3$ and $E_{\text{cav}} = 4 P_s V_c$. However, it was recently indicated that the cavities could be filled with low-energy cosmic rays from the spectra of radio minihalos (Fujita & Ohira 2012, 2013). In that case, γ_c is close to $5/3$ and $E_{\text{cav}} = 2.5 P_s V_c$. Thus, we multiply P_{jet} in McNamara, Rohanizadegan, & Nulsen (2011) by $2.5/4$, although the results are not much affected by this modification. Note that while equation (13) is appropriate for FR I objects (most of our sample galaxies), it may underestimate the jet power for FR II objects (Cygnus A) at most a factor of 10 (Ito et al. 2008). Thus, P_{jet} for Cygnus A should be regarded as a lower-limit.

We present P_{jet} and P_B in Tables 2 and 3, and display their relationship in Fig. 2. A positive correlation between P_{jet} and P_B can be clearly seen. We found that the Spearman's rank coefficient is 0.47. The probability that this is produced from a random distribution is $P_{\text{null}} = 1.2 \times 10^{-2}$. Using an ordinary least-squares bisector regression method (Isobe et al. 1990) and the code³, the correlation can be described as a power-law model of the form

$$\log \frac{P_{\text{jet}}}{10^{42} \text{ erg s}^{-1}} = A_1 + B_1 \log \frac{P_B}{10^{42} \text{ erg s}^{-1}}, \quad (14)$$

where $A_1 = -1.65_{-1.09}^{+1.57}$ and $B_1 = 1.14_{-0.22}^{+0.09}$. The uncertainties were estimated by the Monte Carlo simulations. Fig. 3 shows that $P_{\text{jet}}/P_B \lesssim 1$ except for Hercules A ($P_{\text{jet}}/P_B = 20$), which means that the Bondi accretion can power the jet activities in general, contrary to previous studies (McNamara, Rohanizadegan, & Nulsen 2011). Note that P_{jet}/P_B we obtained are much smaller than those in Fig. 2 of McNamara, Rohanizadegan, & Nulsen (2011), because they used the gas density and temperature at $r = r_{\text{obs}}$ and thus their resulting \dot{M}_B is generally smaller than ours. Except for Hercules A, the power ratios are in the range of $10^{-3} \lesssim P_{\text{jet}}/P_B \lesssim 1$ and $\eta P_{\text{jet}}/P_B$ shows the energy conversion efficiency from the rest mass energy of the infalling gas to the jet power. The reason why Hercules A exhibits a ratio that high can be related to the ongoing merger detected by the *Hubble Space Telescope* (O'Dea et al. 2013), supplemented by injection of the cold dusty gas in the region of r_B causing the hydrostatic equilibrium to be strongly perturbed.

5 DISCUSSION

The correlation between P_{jet} and P_B shown in Fig. 2 and the fact that $P_{\text{jet}}/P_B \lesssim 1$, as shown in Fig. 3, indicate that

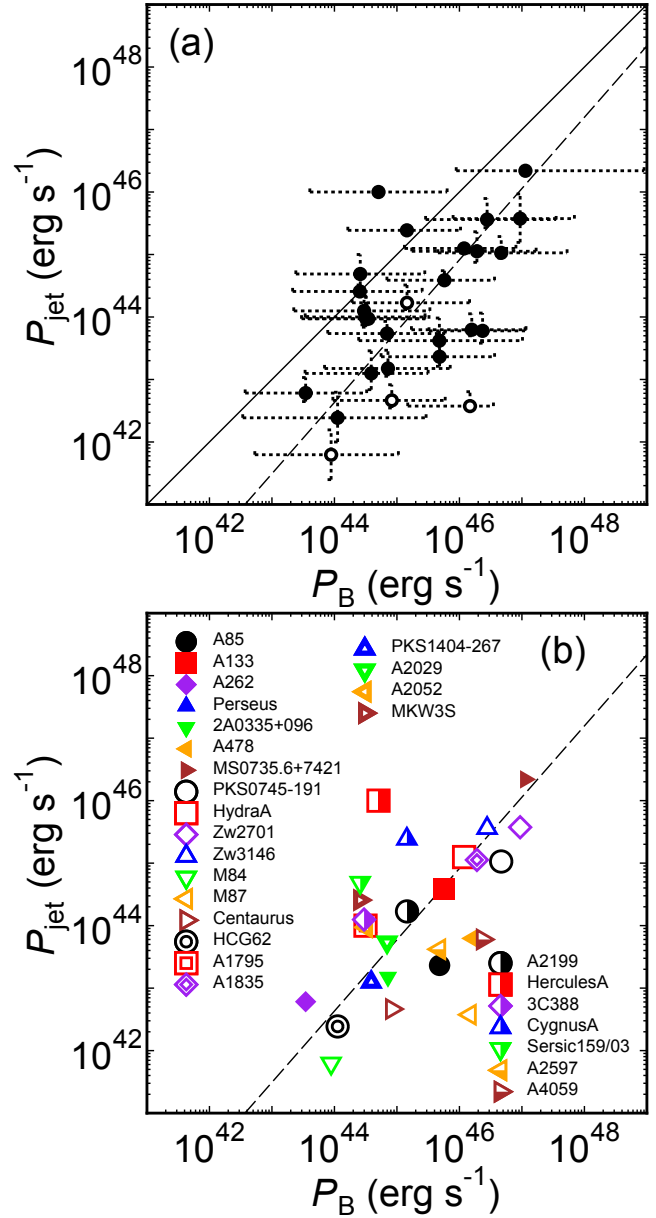


Figure 2. (a) Relation between Bondi power P_B and jet power P_{jet} . The dashed-line is the best fitting model represented by equation (14). The solid line is $P_{\text{jet}} = P_B$. The open circles are the galaxies studied by Allen et al. (2006). (b) Same as (a) but object names are shown instead of error bars.

the SMBH jet activities of are controlled by accretion of the ambient hot gas. This leads to the stable suppression of the cooling flows in cluster cores (Section 1). The correlation in Fig. 2 has a large scatter. This may be partly related to the uncertainties of observations. Allen et al. (2006) studied 9 nearby X-ray luminous elliptical galaxies and found a tight $P_{\text{jet}}-P_B$ correlation. However, Russell et al. (2013), based on the revised analysis, indicated that the correlation is much weaker. Our sample contains four galaxies studied by Allen et al. (2006) — M86, M87, NGC 4696 (Centaurus), and NGC 6166 (A2199). The correlation among the four galaxies in Fig. 2a is not as tight as that in Fig. 4 of Allen et al. (2006). While Allen et al. (2006) studied the

³ http://astrostatistics.psu.edu/statcodes/sc_regression.html

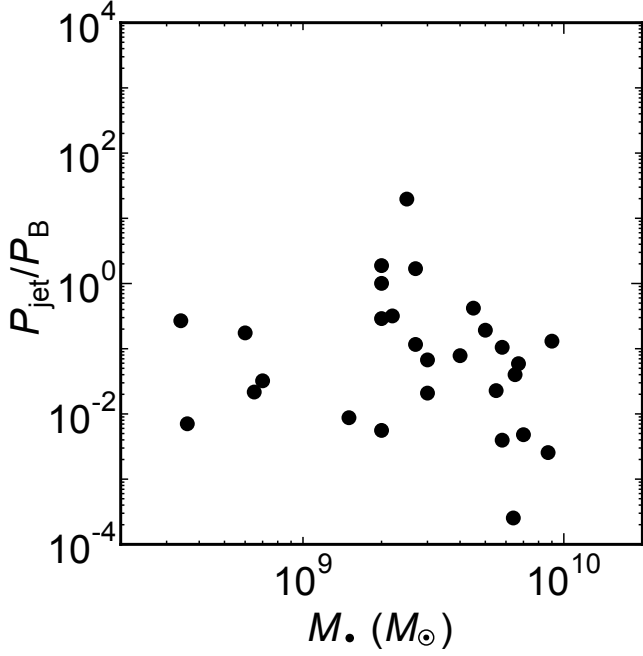


Figure 3. Relation between the mass of SMBHs M_\bullet and the ratio of the jet power P_{jet} to the Bondi accretion power P_B . Error bars are omitted for clarity.

$P_{\text{jet}}-P_B$ relation over 2.5 orders of magnitude in P_{jet} , we studied the relation over 4 orders of magnitude (Fig. 2), which may be the reason that we found the correlation in spite of the large scatter.

Uncertainties in our model may also be responsible for the scatter. In the case of the Centaurus, for example, we predict that the gas density continues to increase and the temperature is nearly constant toward r_B (Fig. 1). On the contrary, the latest *Chandra* observations detected a flatter density profile and a slightly rising temperature at $r \lesssim 1$ kpc (Russell et al. 2013), which may be due to gas heating by the AGN. This heating may cause \dot{M}_B to decrease at r_B . For the Perseus cluster, *Chandra* observations have shown that the temperature seems to bottom out at ~ 3 keV instead of $T_0 \sim 1$ keV, and that the central region ($\lesssim 10$ kpc) is strongly disturbed by the cavities (Fabian et al. 2006).

Equation (1) shows that the Bondi accretion rate \dot{M}_B is determined by M_\bullet , ρ_B and T_B . The correlations between M_\bullet and P_B , and between $n_{e,B}$ and P_B are noticeable (Figs. 4a and 4b). On the other hand, there is no correlation between T_B and P_B , and between M_\bullet and $n_{e,B}$ (Figs. 4c and 4d). Therefore, the latter two parameters affect \dot{M}_B independently. Since $n_{e,B}$ depends on n_{obs} , the jet activity may be regulated by their past gas heating at $r \gtrsim r_{\text{obs}}$. No detection of correlation between T_B and P_B (Fig. 4c) results from the scatter of T_0 among our sample galaxies being small.

Studies have indicated that the properties of the accretion disc around a SMBH depend on the gas accretion rate normalised by the Eddington accretion rate (Narayan & McClintock 2008; Yuan & Narayan 2014),

$$\dot{M}_{\text{Edd}} = L_{\text{Edd}}/(\eta_r c^2), \quad (15)$$

where $\eta_r = 0.1$ is the radiation efficiency, and L_{Edd} is the Eddington luminosity:

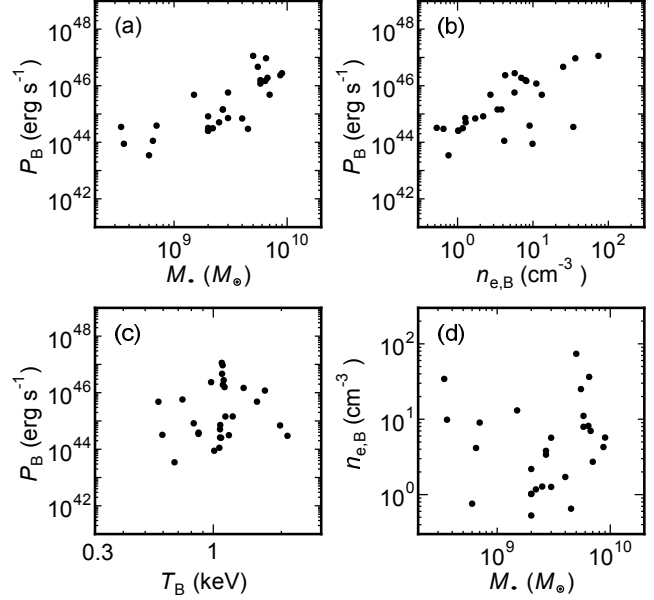


Figure 4. (a) Mass of the SMBH M_\bullet vs. Bondi accretion power P_B . (b) Electron density at the Bondi radius $n_{e,B}$ vs. Bondi accretion power P_B . (c) Temperature at the Bondi radius T_B vs. Bondi accretion power P_B . (d) Mass of the SMBH M_\bullet vs. electron density at the Bondi radius $n_{e,B}$. Error bars are omitted for clarity.

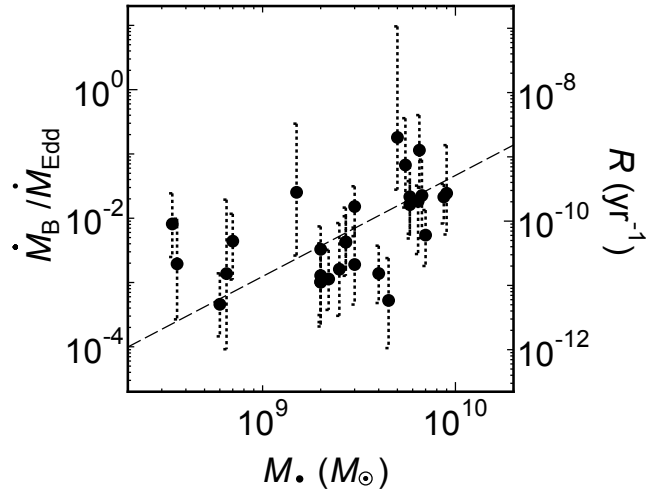


Figure 5. Mass of the SMBHs M_\bullet vs. Eddington-scaled Bondi accretion rate $\dot{M}_B/\dot{M}_{\text{Edd}}$ or specific growth rate $\mathcal{R} = \dot{M}_B/M_\bullet$. The dashed-line is the best fitting model represented by equation (17).

$$L_{\text{Edd}} = 1.26 \times 10^{38} \left(\frac{M_\bullet}{M_\odot} \right) \text{ erg s}^{-1} \quad (16)$$

(e.g. Narayan & McClintock 2008). In Fig. 5, we show a plot of M_\bullet versus $\dot{M}_B/\dot{M}_{\text{Edd}}$. A positive correlation is seen and the best fitting relation is

$$\log \left(\frac{\dot{M}_B}{\dot{M}_{\text{Edd}}} \right) = A_2 + B_2 \log \left(\frac{M_\bullet}{10^9 M_\odot} \right), \quad (17)$$

where $A_2 = -2.91^{+0.57}_{-0.47}$ and $B_2 = 1.57^{+0.45}_{-0.18}$. The probability that this is produced from a random distribution is

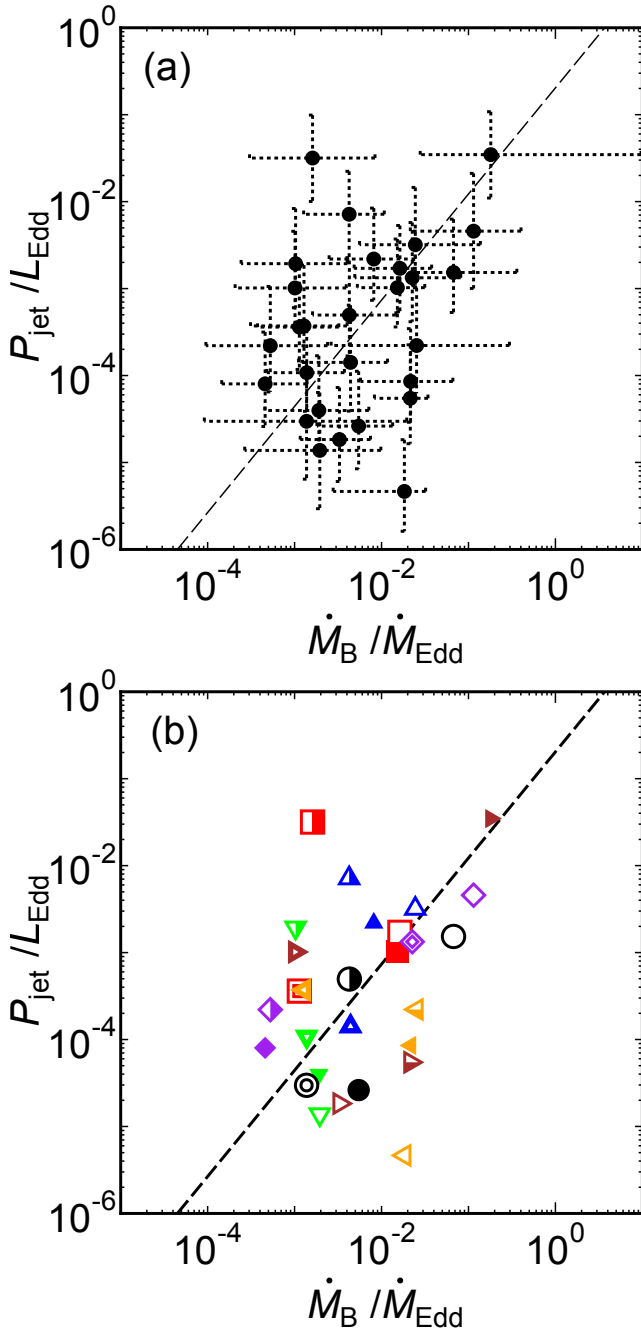


Figure 6. (a) Relation between Eddington-scaled Bondi accretion rate $\dot{M}_B/\dot{M}_{\text{Edd}}$ and Eddington-scaled jet power $P_{\text{jet}}/L_{\text{Edd}}$. The dashed-line is the best fitting model represented by equation (18). (b) Same as (a) but object names are shown by the marks in Fig. 2b.

only $P_{\text{null}} = 1.8 \times 10^{-3}$. The positive correlation reflects the relation between M_\bullet and P_B shown in Fig. 4a. This is in contrast with the trend for $\sim 23,000$ type 2 AGNs in the Sloan Digital Sky Survey (SDSS). Heckman et al. (2004) indicated that most present-day accretion occurs onto SMBHs with masses less than $10^8 M_\odot$, and the accretion onto more massive SMBHs is inefficient and, therefore, substantially sub-Eddington.

A simple explanation can be that the hot accretion flows

in BCGs are maintained by continuous heating from the AGN. The gas accretion rate normalised by the Eddington accretion rate $\dot{M}_B/\dot{M}_{\text{Edd}}$ is proportional to the black hole specific growth rate $\mathcal{R} = \dot{M}_B/M_\bullet$. Fig. 5 shows that the growth timescale (\mathcal{R}^{-1}) is smaller than the age of the galaxies (~ 10 Gyr) for $M_\bullet \gtrsim 3 \times 10^9 M_\odot$, and the specific growth rate for the most massive SMBHs ($\sim 10^{10} M_\odot$) is $\mathcal{R} \sim 0.5 \text{ Gyr}^{-1}$. Although it is not certain whether the high accretion rates are maintained for a long time, they might have caused rapid growth of those SMBHs. This accretion may lead to the formation of SMBHs with $M_\bullet \sim 10^{10} M_\odot$.

Fig. 6 shows the relation between $\dot{M}_B/\dot{M}_{\text{Edd}}$ and $P_{\text{jet}}/L_{\text{Edd}}$. The best fitting relation is

$$\log\left(\frac{P_{\text{jet}}}{L_{\text{Edd}}}\right) = A_3 + B_3 \log\left(\frac{\dot{M}_B}{\dot{M}_{\text{Edd}}}\right), \quad (18)$$

where $A_3 = -0.69^{+0.76}_{-1.18}$ and $B_3 = 1.22^{+0.04}_{-0.25}$. However, the null probability is relatively large, i.e., $P_{\text{null}} = 0.15$. Thus, Fig 6 displays that $P_{\text{jet}}/L_{\text{Edd}}$ has a large scatter for a given $\dot{M}_B/\dot{M}_{\text{Edd}}$. The poor correlation among the above scaled values means that the relation between P_B and P_{jet} in Fig. 2 does not depend on the black hole mass alone (see also Fig. 3). Moreover, the underlying accretion disk properties and the jet production efficiency do not depend only on $\dot{M}_B/\dot{M}_{\text{Edd}}$.

We also found that the AGN luminosities do not necessarily increase with the accretion rate ratio $\dot{M}_B/\dot{M}_{\text{Edd}}$. In Fig. 7, we present a plot of $\dot{M}_B/\dot{M}_{\text{Edd}}$ versus L_X/L_{Edd} , where L_X is the X-ray luminosity derived from the X-ray flux obtained by Russell et al. (2013), except for Perseus (Table 2). The X-ray flux from the AGN in the Perseus cluster is too large to measure accurately (Russell et al. 2013), and it is not included in the figure. Fig. 7 shows that the AGN are very dim and for most of them only upper limits have been obtained. The dashed line is the relation represented by

$$\frac{L_X}{L_{\text{Edd}}} = \frac{\dot{M}_B}{\dot{M}_{\text{Edd}}} \quad (19)$$

for $\dot{M}_B/\dot{M}_{\text{Edd}} > 0.01$ and

$$\frac{L_X}{L_{\text{Edd}}} = 100 \left(\frac{\dot{M}_B}{\dot{M}_{\text{Edd}}}\right)^2 \quad (20)$$

for $\dot{M}_B/\dot{M}_{\text{Edd}} < 0.01$, which is often applied to stellar-mass black holes in the Galaxy (e.g. Narayan & McClintock 2008). Fig. 7 shows that all the AGN in our sample are much dimmer than that relation and they are extremely radiatively inefficient, especially when compared to the X-ray binaries (e.g. Esin, McClintock, & Narayan 1997). Although some of the non-detected sources could be heavily absorbed, it is unlikely that the absorption alone can explain the overall dimness of the AGN (Russell et al. 2013). The dimness of the AGNs in elliptical galaxies has also been pointed out in previous studies (Di Matteo et al. 2000; Loewenstein et al. 2001; Pellegrini 2005; Balmaverde, Baldi, & Capetti 2008). Fig. 7 shows that some galaxies have accretion rates that are even larger than $\dot{M}_B/\dot{M}_{\text{Edd}} = 0.01$, above which the accretion discs are expected to become radiatively efficient (Narayan & McClintock 2008; Yuan & Narayan 2014). Their low X-ray luminosities shown in Fig. 7 may indicate that $\dot{M}_B/\dot{M}_{\text{Edd}}$ is not the only parameter that deter-

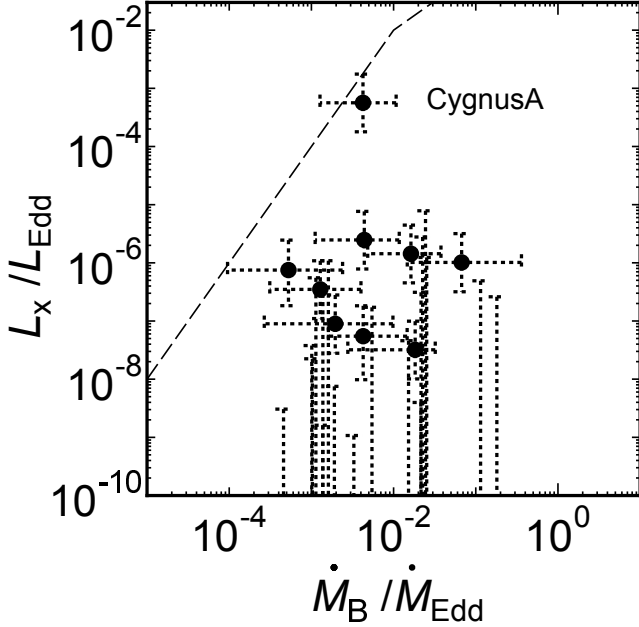


Figure 7. Eddington-scaled Bondi accretion rate $\dot{M}_B/\dot{M}_{\text{Edd}}$ and Eddington-scaled X-ray luminosity L_X/L_{Edd} . The dashed-line is a relation for X-ray binaries represented by equations (19) and (20).

mines the radiative efficiency of accretion discs. BCGs at low-redshifts are immersed in the hot intracluster medium (ICM), which is being continuously heated by the AGN (otherwise cooling flows should have developed). Within this framework, the hot gas accretion may dominate and radiatively inefficient accretion may be allowed even if $\dot{M}_B/\dot{M}_{\text{Edd}} \gtrsim 0.01$. The statistical significance of the above effect, however, is not clear, as only 3 galaxies (MS 0735.6+7421, PKS 0745-191, and Zw 2701) exceed accretion rates $\dot{M}_B/\dot{M}_{\text{Edd}} \sim 0.01$ by more than 1σ .

Fig. 8 shows the Bondi accretion power (P_B) and the X-ray luminosity of the ICM inside the cluster cooling radius that is offset to be consistent with the spectra ($L_{\text{ICM}} = L_{\text{Xc}} - L_{\text{cool}}$). The luminosities are derived by Rafferty et al. (2006); L_{Xc} is the X-ray luminosity within which the gas has a cooling time less than 7.7×10^9 yr (the look-back time for $z = 1$), and L_{cool} is the associated (cooling) luminosity of gas cooling to low temperatures, derived from the X-ray spectrum. Since L_{cool} could not be determined for A1835 (Rafferty et al. 2006), we assume $L_{\text{cool}} = 0$ for the cluster. However, since $L_{\text{cool}} \ll L_{\text{Xc}}$ for most other clusters, the assumption will not affect the results strongly.

Fig. 8 indicates that P_B and L_{ICM} are tightly correlated. It suggests strongly that the radiative energy loss of the cluster cool cores is being compensated by the AGN feedback. The best fitting relation is

$$\log \left(\frac{L_{\text{ICM}}}{10^{42} \text{ erg s}^{-1}} \right) = A_4 + B_4 \log \left(\frac{P_B}{10^{42} \text{ erg s}^{-1}} \right), \quad (21)$$

where $A_4 = -1.28_{-0.97}^{+1.31}$ and $B_4 = 1.04_{-0.19}^{+0.07}$. The null probability is $P_{\text{null}} = 3.1 \times 10^{-3}$. The index B_4 is consistent with unity, which means that P_B is proportional to L_{ICM} . The fact that $L_{\text{ICM}}/P_B \lesssim 1$ means that the Bondi accretion power is large enough to offset radiative cooling of the cool cores.

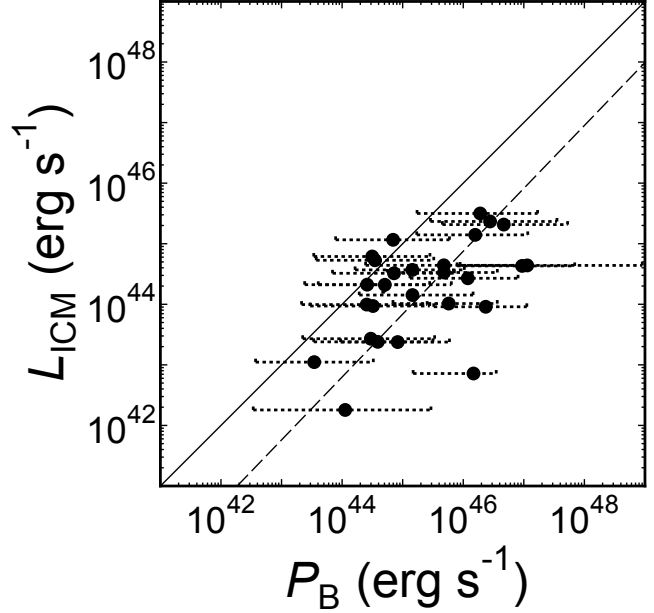


Figure 8. Relation between Bondi power P_B and X-ray luminosity of the cool core L_{ICM} . The errors of L_{ICM} are comparable or smaller than the sizes of the filled circles. The dashed-line is the best fitting model represented by equation (21). The solid line shows $L_{\text{ICM}} = P_B$.

Since $L_{\text{ICM}}/P_B \sim 0.1$ on average and $\eta = 0.1$, about 1% of the rest mass energy of the accreted gas that passed r_B was used to heat up the cool cores. The correlation described by equation (21) may reflect the fact that lower entropy (higher density and/or lower temperature) of the gas leads to both larger \dot{M}_B (equation 1) and larger L_{ICM} . However, since \dot{M}_B is also sensitive to M_\bullet and $g(r)$ (equation 7), the correlation is not obvious.

Fujita & Reiprich (2004) showed that no correlation exists between M_\bullet and L_{ICM} . This may indicate that the accretion rate fluctuates with time. Birzan et al. (2004) and Rafferty et al. (2006) compare P_{jet} with L_{ICM} and found a correlation between them. However, for a significant fraction of their sample clusters, they have shown that $P_{\text{jet}} < L_{\text{ICM}}$, which may mean that the jet power alone is not large enough to balance the cooling. Combining the relation $P_{\text{jet}} \lesssim L_{\text{ICM}}$ with our results $P_{\text{jet}} \lesssim P_B$ (Fig. 3) and $P_B \gtrsim L_{\text{ICM}}$ (Fig. 8), we obtain $P_{\text{jet}} \lesssim L_{\text{ICM}} \lesssim P_B$. Assuming that L_{ICM}/P_B of the Bondi power is used to heat the cool core, a large portion of the Bondi power ($\sim (L_{\text{ICM}} - P_{\text{jet}})/P_B$) may be transferred to the ICM through the form that does not appear in the jet power P_{jet} estimated from the cavity volumes (equation 13). This energy can be transferred by the cosmic rays escaping from the cavities (Guo & Oh 2008; Fujita & Ohira 2013). However, since the AGN activities are intermittent, time-averaged jet power \bar{P}_{jet} may be close to the ICM luminosity L_{ICM} . It is also likely that not all cavities have been observed, and that P_{jet} has been underestimated.

The discussions so far are based on the Bondi accretion (Bondi 1952). However, whether the Bondi accretion is actually realised in galaxies have been debated in the literature. For example, small angular momentum of the accreting gas may significantly reduce the accretion rate by introducing a centrifugal barrier (Proga & Begelman 2003;

Krumholz, McKee, & Klein 2005), although viscosity of the hot gas may transport the angular momentum (Park 2009; Inogamov & Sunyaev 2010; Narayan & Fabian 2011). Moreover, owing to the high density and the short cooling time of the hot gas around the SMBH, thermal instability may develop there and a substantial fraction of the hot gas may turn into cold gas (Soker 2006; Barai, Proga, & Nagamine 2012; Sharma et al. 2012; Gaspari, Ruszkowski, & Oh 2013). It is interesting to note that even if this happens, the apparent X-ray temperature does not necessarily decrease near the galactic centre, in spite of the efficient cooling (Gaspari, Ruszkowski, & Oh 2013). *Chandra* observations show that the hot gas density drops while its temperature is almost constant at $\lesssim 10$ kpc from the centre of the Perseus cluster (Fabian et al. 2006). Although the density profile might have been affected by the hot cavities or temporal AGN heating, it could also be the result of the removal of the hot gas by the thermal instability which triggers a cold gas flow in the region. The angular momentum initially retained by turbulent hot gas may decrease after the development of the thermal instability through collisions between cold blobs (Shlosman et al. 1990), which can also lead to the formation of a turbulent cold disk and develop a large accretion rate at the event horizon of the black hole \dot{M}_{BH} (Pizzolato & Soker 2010; Gaspari et al. 2014). Furthermore, outflows may significantly modify the accretion flow and may make \dot{M}_{BH} much smaller than the apparent Bondi accretion rate \dot{M}_{B} (Blandford & Begelman 1999; Yuan, Bu, & Wu 2012). If $\dot{M}_{\text{BH}} \ll \dot{M}_{\text{B}}$, other energy sources such as black hole spins are required for efficient jet production (Nemmen & Tchekhovskoy 2014). On the other hand, outflows can solve the problem of low radiative efficiency of the SMBHs (Fig. 7), because L_{X} should reflect \dot{M}_{BH} , which could be much smaller than \dot{M}_{B} .

The correlations found in this study do not necessarily mean that the accretion flows in BCGs are represented by the ‘classical’ and oversimplified Bondi accretion flow. Significant departures from such a flow, which involve angular momentum, multi-phase gas, and time- and space-averaging should be expected. Hence the hot gas accretion flows appear to reflect the Bondi model in some broad sense. At least, it reflects the density and temperature (or entropy) of the hot gas at $r \sim r_{\text{obs}}$ ($\sim 1\text{--}70$ kpc; Table 2), because we estimated r_{B} and \dot{M}_{B} from them. For example, the thermal instability turns on at some radius $r_{\text{inst}} (< r_{\text{obs}})$, and the emerging cold gas flow ($r \lesssim r_{\text{inst}}$) is influenced by the boundary conditions at $r \sim r_{\text{obs}}$.

6 CONCLUSIONS

We have investigated the Bondi accretion onto the SMBHs in BCGs. For that purpose, we devised a new method to estimate the Bondi accretion rate even when the Bondi radius is under-resolved in the X-ray observations. Our method is based on two assumptions: (1) the gas is in nearly a hydrostatic equilibrium, and (2) the gas temperature is represented by the virial temperature of the galaxy near its centre.

We have applied our method to 28 galaxies and have obtained the Bondi accretion rates. We found a correlation between the Bondi accretion power and the power of the

jets associated with the SMBHs. We also found that the jet power can be well supported by the Bondi accretion, in contrast with previous studies. These results indicate that the AGN feedback in the BCGs is controlled by the accretion of the surrounding hot gas, whose origin lies in a stable heating of the cluster cool cores. The specific growth rates of the SMBHs increase as their mass increases, which may explain the existence of hypermassive SMBHs ($\sim 10^{10} M_{\odot}$). The Eddington X-ray luminosities of the AGN are very small compared to their Eddington luminosities, even if the accretion rates are close to the Eddington accretion rate. This may suggest that massive gas accretion with a low radiative efficiency is realised in BCGs. Moreover, we have found that the Bondi accretion power correlates linearly with the X-ray luminosities of the cluster cool cores. We have shown that the power is large enough to offset the radiative cooling of the cool core. These results may indicate that the cooling of the cool cores is well balanced with the AGN feedback associated with the Bondi accretion.

While the correlations we found do not necessarily mean that the gas accretion on the SMBHs in BCGs follows the simplified Bondi prescription, they demonstrate that the accretion onto the SMBHs follows it in the broad sense, in some time- and space-averaged sense.

ACKNOWLEDGMENTS

We are grateful to the referee for valuable comments. We thank M. Gaspari, Y. Kunisawa, K. Nagamine, N. Soker, and F. Yuan for useful discussions. This work was supported by International Joint Research Promotion Program by Osaka University. NK acknowledges the financial support of Grant-in-Aid for Young Scientists (B:25800099). I.S. acknowledges partial support from the NSF and STScI. STScI is operated by AURA, Inc., under NASA contract NAS 5-26555.

REFERENCES

- Allen S. W., Dunn R. J. H., Fabian A. C., Taylor G. B., Reynolds C. S., 2006, *MNRAS*, 372, 21
- Balmaverde B., Baldi R. D., Capetti A., 2008, *A&A*, 486, 119
- Barai P., Proga D., Nagamine K., 2012, *MNRAS*, 424, 728
- Best P. N., Kaiser C. R., Heckman T. M., Kauffmann G., 2006, *MNRAS*, 368, L67
- Birzan L., Rafferty D. A., McNamara B. R., Wise M. W., Nulsen P. E. J., 2004, *ApJ*, 607, 800
- Blandford R. D., Begelman M. C., 1999, *MNRAS*, 303, L1
- Bondi H., 1952, *MNRAS*, 112, 195
- Bower R. G., Benson A. J., Malbon R., Helly J. C., Frenk C. S., Baugh C. M., Cole S., Lacey C. G., 2006, *MNRAS*, 370, 645
- Bryan G. L., Norman M. L., 1998, *ApJ*, 495, 80
- David L. P., Nulsen P. E. J., McNamara B. R., Forman W., Jones C., Ponman T., Robertson B., Wise M., 2001, *ApJ*, 557, 546
- Di Matteo T., Quataert E., Allen S. W., Narayan R., Fabian A. C., 2000, *MNRAS*, 311, 507
- Edge A. C., 2001, *MNRAS*, 328, 762

- Esin A. A., McClintock J. E., Narayan R., 1997, *ApJ*, 489, 865
- Ettori S., De Grandi S., Molendi S., 2002, *A&A*, 391, 841
- Ettori S., Gastaldello F., Leccardi A., Molendi S., Rossetti M., Buote D., Meneghetti M., 2010, *A&A*, 524, A68
- Fabian A. C., Sanders J. S., Taylor G. B., Allen S. W., Crawford C. S., Johnstone R. M., Iwasawa K., 2006, *MNRAS*, 366, 417
- Fujita Y., et al., 2013, *PASJ*, 65, L15
- Fujita Y., Kimura S., Ohira Y., 2013, *MNRAS*, 432, 1434
- Fujita Y., Ohira Y., 2013, *MNRAS*, 428, 599
- Fujita Y., Ohira Y., 2012, *ApJ*, 746, 53
- Fujita Y., Reiprich T. H., 2004, *ApJ*, 612, 797
- Fujita Y., Suzuki T. K., 2005, *ApJ*, 630, L1
- Gaspari M., Ruszkowski M., Oh S. P., 2013, *MNRAS*, 432, 3401
- Gaspari M., Ruszkowski M., Oh S. P., Brighenti F., Temi P., 2014, *arXiv*, arXiv:1407.7531
- Gizani N. A. B., Leahy J. P., 2004, *MNRAS*, 350, 865
- Guo F., Mathews W. G., 2014, *ApJ*, 780, 126
- Guo F., Oh S. P., 2008, *MNRAS*, 384, 251
- Hamer S. L., et al., 2014, *MNRAS*, 437, 862
- Heckman T. M., Kauffmann G., Brinchmann J., Charlot S., Tremonti C., White S. D. M., 2004, *ApJ*, 613, 109
- Hernquist L., 1990, *ApJ*, 356, 359
- Inogamov N. A., Sunyaev R. A., 2010, *AstL*, 36, 835
- Isobe T., Feigelson E. D., Akritas M. G., Babu G. J., 1990, *ApJ*, 364, 104
- Ito H., Kino M., Kawakatu N., Isobe N., Yamada S., 2008, *ApJ*, 685, 828
- Krumholz M. R., McKee C. F., Klein R. I., 2005, *ApJ*, 618, 757
- Loewenstein M., Mushotzky R. F., Angelini L., Arnaud K. A., Quataert E., 2001, *ApJ*, 555, L21
- Lokas E. L., Wojtak R., Gottlöber S., Mamon G. A., Prada F., 2006, *MNRAS*, 367, 1463
- Makino N., Sasaki S., Suto Y., 1998, *ApJ*, 497, 555
- Mathews W. G., Faltenbacher A., Brighenti F., 2006, *ApJ*, 638, 659
- Matsushita K., 2001, *ApJ*, 547, 693
- McLaughlin D. E., 1999, *ApJ*, 512, L9
- McLure R. J., Dunlop J. S., 2002, *MNRAS*, 331, 795
- McNamara B. R., Nulsen P. E. J., 2007, *ARA&A*, 45, 117
- McNamara B. R., Nulsen P. E. J., Wise M. W., Rafferty D. A., Carilli C., Sarazin C. L., Blanton E. L., 2005, *Natur*, 433, 45
- McNamara B. R., Rohanizadegan M., Nulsen P. E. J., 2011, *ApJ*, 727, 39
- Molikawa K., Hattori M., Kneib J.-P., Yamashita K., 1999, *A&A*, 351, 413
- Narayan R., Fabian A. C., 2011, *MNRAS*, 415, 3721
- Narayan R., McClintock J. E., 2008, *NewAR*, 51, 733
- Navarro J. F., Frenk C. S., White S. D. M., 1996, *ApJ*, 462, 563
- Nemmen R. S., Tchekhovskoy A., 2014, *arXiv*, arXiv:1406.7420
- O'Dea C. P., Baum S. A., Tremblay G. R., Kharb P., Cotton W., Perley R., 2013, *ApJ*, 771, 38
- Park M.-G., 2009, *ApJ*, 706, 637
- Pellegrini S., 2005, *ApJ*, 624, 155
- Piffaretti R., Jetzer P., Kaastra J. S., Tamura T., 2005, *A&A*, 433, 101
- Pizzolato F., Soker N., 2010, *MNRAS*, 408, 961
- Pointecouteau E., Arnaud M., Pratt G. W., 2005, *A&A*, 435, 1
- Proga D., Begelman M. C., 2003, *ApJ*, 582, 69
- Rafferty D. A., McNamara B. R., Nulsen P. E. J., Wise M. W., 2006, *ApJ*, 652, 216
- Richard J., et al., 2010, *MNRAS*, 404, 325
- Russell H. R., McNamara B. R., Edge A. C., Hogan M. T., Main R. A., Vantyghem A. N., 2013, *MNRAS*, 432, 530
- Ruszkowski M., Begelman M. C., 2002, *ApJ*, 581, 223
- Schmidt R. W., Allen S. W., 2007, *MNRAS*, 379, 209
- Sharma P., McCourt M., Quataert E., Parrish I. J., 2012, *MNRAS*, 420, 3174
- Shlosman, I., Begelman, M.C., Frenk, J., 1990, *Nature*, 345, 679
- Smith D. A., Wilson A. S., Arnaud K. A., Terashima Y., Young A. J., 2002, *ApJ*, 565, 195
- Soker N., 2006, *NewA*, 12, 38
- Sun M., Voit G. M., Donahue M., Jones C., Forman W., Vikhlinin A., 2009, *ApJ*, 693, 1142
- Vattakunnel S., Trussoni E., Capetti A., Baldi R. D., 2010, *A&A*, 522, A89
- Vikhlinin A., Kravtsov A., Forman W., Jones C., Markevitch M., Murray S. S., Van Speybroeck L., 2006, *ApJ*, 640, 691
- Werner N., et al., 2014, *MNRAS*, 439, 2291
- Wojtak R., Lokas E. L., 2010, *MNRAS*, 408, 2442
- Yuan F., Bu D., Wu M., 2012, *ApJ*, 761, 130
- Yuan F., Narayan R., 2014, *arXiv*, arXiv:1401.0586

Table 1. Parameters for Gravitational Potentials

System	z	M_{\bullet} ($10^9 M_{\odot}$)	M_{gal} ($10^{11} M_{\odot}$)	R_e (kpc)	σ (km s^{-1})	c_{vir}	M_{vir} ($10^{14} M_{\odot}$)	References ^a
A85	0.055	7.0	31.0 ± 1.0	16.3 ± 0.03	348.4 ± 18.6	$4.25^{+0.76}_{-0.96}$	$12.33^{+1.78}_{-1.34}$	1
A133	0.060	3.0	17.9 ± 0.4	14.6 ± 0.43	236.2 ± 11.4	$6.35^{+0.53}_{-0.53}$	$5.64^{+0.88}_{-0.77}$	2
A262	0.016	0.6	4.9 ± 0.1	10.4 ± 0.58	229.8 ± 9.7	$8.84^{+0.69}_{-0.69}$	$1.15^{+0.092}_{-0.15}$	3
Perseus	0.018	0.34	19.2 ± 0.1	11.3 ± 0.43	258.9 ± 13.4	$8.08^{+0.35}_{-0.35}$	$6.81^{+0.63}_{-0.72}$	4
2A 0335+096	0.035	3.0	18.0 ± 1.0	15.0 ± 1.4	289.5 ± 35.9	$7.44^{+0.42}_{-0.42}$	$2.11^{+0.24}_{-0.29}$	3
A478	0.081	5.8	28.0 ± 1.0	15.8 ± 3.1	289.5 ± 35.9	$5.15^{+0.45}_{-0.49}$	$16.6^{+2.0}_{-2.6}$	5
MS 0735.6+7421	0.216	5.0	24.0 ± 1.0	15.1 ± 3.8	289.5 ± 35.9	$8.41^{+8.37}_{-4.20}$	$25^{+24.9}_{-12.5}$	6
PKS 0745-191	0.103	5.5	27.0 ± 1.0	16.1 ± 3.3	289.5 ± 35.9	$7.75^{+2.15}_{-1.41}$	$14.9^{+6.7}_{-3.7}$	5
Hydra A	0.055	5.8	28.2 ± 0.7	10.5 ± 0.90	361.9 ± 19.1	$15.90^{+1.23}_{-0.23}$	$1.15^{+3.7}_{-0.36}$	7
Zw 2701	0.214	6.5	30.0 ± 1.0	13.4 ± 1.3	289.5 ± 35.9	$3.30^{+1.2}_{-1.2}$	$10.86^{+2.57}_{-5.86}$	8
Zw 3146	0.291	9.0	13.5 ± 6.9	17.4 ± 7.6	289.5 ± 35.9	$4.19^{+0.18}_{-0.31}$	$9.29^{+1.04}_{-0.55}$	9
M84	0.0035	0.36	4.3 ± 1.3	2.45 ± 0.06	282.4 ± 2.6
M87	0.0042	6.4	11.0 ± 3.3	3.67 ± 0.13	336.4 ± 4.6	$3.84^{+0.91}_{-0.92}$	$5.78^{+0.59}_{-1.5}$	10
Centaurus	0.011	2.0	11.6 ± 0.1	9.44 ± 0.24	254.2 ± 7.3	$7.75^{+0.77}_{-0.78}$	$4.09^{+0.32}_{-0.62}$	4
HCG 62	0.014	0.65	13.5 ± 6.9	6.87 ± 0.04	289.5 ± 35.9
A1795	0.063	2.2	13.4 ± 0.6	20.8 ± 0.23	302.0 ± 8.7	$6.16^{+1.14}_{-1.14}$	$10.8^{+2.7}_{-2.4}$	5
A1835	0.253	6.7	13.5 ± 6.9	18.4 ± 0.35	289.5 ± 35.9	$4.18^{+0.63}_{-0.41}$	$24.3^{+4.4}_{-4.9}$	5
PKS 1404-267	0.022	0.7	5.7 ± 0.5	6.03 ± 0.12	259.7 ± 6.5	$12.25^{+1.09}_{-6.07}$	$1.77^{+0.43}_{-0.31}$	1
A2029	0.077	4.0	21.9 ± 0.2	24.2 ± 1.6	390.8 ± 10.0	$8.86^{+0.44}_{-0.50}$	$10.1^{+0.99}_{-0.77}$	5
A2052	0.035	2.0	11.0 ± 3.3	15.7 ± 0.27	215.8 ± 11.6	$6.50^{+0.71}_{-0.71}$	$2.96^{+0.52}_{-0.77}$	3
MKW 3S	0.045	2.0	11.2 ± 0.3	11.6 ± 2.3	289.5 ± 35.9	$7.83^{+0.55}_{-0.55}$	$2.90^{+0.27}_{-0.38}$	3
A2199	0.030	2.7	15.7 ± 0.2	10.6 ± 0.20	307.1 ± 6.9	$10.40^{+14.6}_{-7.9}$	$7.1^{+3.4}_{-2.4}$	11
Hercules A	0.154	2.5	15.0 ± 4.0	20.1 ± 2.0	289.5 ± 35.9	$3.51^{+0.23}_{-0.23}$	$4.33^{+0.54}_{-0.54}$	12,13
3C 388	0.092	4.5	23.0 ± 6.0	11.9 ± 1.2	408.3 ± 25.7
Cygnus A	0.056	2.7	9.0 ± 2.0	15.6 ± 0.77	289.5 ± 35.9	$16.40^{+0.25}_{-0.25}$	$8.33^{+0.38}_{-0.38}$	13,14
Sersic 159/03	0.058	2.0	11.0 ± 2.0	20.2 ± 0.95	289.5 ± 35.9	$8.57^{+0.69}_{-0.69}$	$1.61^{+0.12}_{-0.20}$	3
A2597	0.085	1.5	9.0 ± 1.0	11.7 ± 1.3	210.0 ± 57.1	$7.60^{+0.63}_{-0.63}$	$3.55^{+0.43}_{-0.40}$	15
A4059	0.048	8.7	38.2 ± 0.4	18.7 ± 0.10	272.1 ± 12.9	$3.57^{+0.68}_{-0.96}$	$4.45^{+0.63}_{-0.62}$	1

^a References for cluster parameters. (1) Wojtak & Lokas (2010); (2) Vikhlinin et al. (2006); (3) Piffaretti et al. (2005); (4) Ettori, De Grandi, & Molendi (2002); (5) Schmidt & Allen (2007); (6) Molikawa et al. (1999); (7) David et al. (2001); (8) Richard et al. (2010); (9) Ettori et al. (2010); (10) McLaughlin (1999); (11) Lokas et al. (2006); (12) Gizani & Leahy (2004), Sun et al. (2009); (14) Smith et al. (2002); (15) Pointecouteau, Arnaud, & Pratt (2005)

Table 2. Observational Data

System	r_{obs} (kpc)	$n_{\text{e,obs}}$ (cm^{-3})	T_{obs} (keV)	P_{jet} ($10^{42} \text{ erg s}^{-1}$)	L_X ($10^{40} \text{ erg s}^{-1}$)	L_{ICM} ($10^{42} \text{ erg s}^{-1}$)
A85	5.8	$0.107^{+0.009}_{-0.008}$	$2.1^{+0.1}_{-0.2}$	23^{+23}_{-7}	< 15	335^{+21}_{-29}
A133	8.0	$0.048^{+0.004}_{-0.005}$	$1.8^{+0.1}_{-0.1}$	387^{+162}_{-13}	< 1.73	103^{+3}_{-3}
A262	3.4	$0.065^{+0.008}_{-0.007}$	$0.86^{+0.01}_{-0.01}$	$6.1^{+4.7}_{-1.6}$	< 0.02	$11.10^{+0.32}_{-0.46}$
Perseus	8.6	$0.150^{+0.005}_{-0.005}$	$4.4^{+0.5}_{-0.4}$	94^{+63}_{-19}	\dots	533^{+7}_{-8}
2A 0335+096	5.1	$0.056^{+0.003}_{-0.002}$	$1.4^{+0.1}_{-0.1}$	15^{+14}_{-4}	< 0.28	325^{+5}_{-4}
A478	5.3	$0.20^{+0.01}_{-0.02}$	$2.7^{+0.3}_{-0.3}$	63^{+50}_{-13}	< 23	1400^{+23}_{-51}
MS 0735.6+7421	23.8	$0.067^{+0.002}_{-0.003}$	$3.2^{+0.2}_{-0.2}$	21900	< 17	438^{+12}_{-16}
PKS 0745-191	11.2	$0.14^{+0.01}_{-0.01}$	$2.6^{+0.4}_{-0.4}$	1060^{+875}_{-188}	71^{+5}_{-11}	2070^{+127}_{-122}
Hydra A	4.7	$0.15^{+0.01}_{-0.02}$	$2.6^{+0.8}_{-0.5}$	1250^{+31}_{-31}	105^{+6}_{-5}	269^{+5}_{-4}
Zw 2701	37.6	$0.024^{+0.002}_{-0.002}$	$3.3^{+0.3}_{-0.3}$	3750^{+5560}_{-2190}	< 40	430^{+18}_{-32}
Zw 3146	15.0	$0.177^{+0.007}_{-0.007}$	$3.1^{+0.3}_{-0.2}$	3620^{+4250}_{-938}	< 891	2330^{+165}_{-193}
M84	0.9	$0.105^{+0.007}_{-0.007}$	$0.57^{+0.01}_{-0.01}$	$0.6^{+0.9}_{-0.4}$	$0.41^{+0.03}_{-0.08}$	$0.06^{+0.01}_{-0.01}$
M87	1.0	$0.191^{+0.009}_{-0.009}$	$0.94^{+0.02}_{-0.02}$	$3.8^{+2.6}_{-0.6}$	$2.58^{+0.16}_{-0.16}$	$7.20^{+0.20}_{-0.11}$
Centaurus	1.3	$0.23^{+0.01}_{-0.01}$	$0.77^{+0.01}_{-0.01}$	$4.6^{+3.6}_{-1.1}$	< 0.03	$23.80^{+0.36}_{-0.36}$
HCG 62	2.1	$0.057^{+0.007}_{-0.005}$	$0.67^{+0.01}_{-0.01}$	$2.4^{+3.8}_{-1.4}$	< 0.01	$1.80^{+0.17}_{-0.25}$
A1795	9.5	$0.067^{+0.005}_{-0.005}$	$2.7^{+0.6}_{-0.4}$	100^{+144}_{-31}	< 15	615^{+9}_{-18}
A1835	27.2	$0.110^{+0.003}_{-0.003}$	$4.0^{+0.3}_{-0.3}$	1120^{+1190}_{-375}	< 235	3160^{+59}_{-89}
PKS 1404-267	8.5	$0.046^{+0.002}_{-0.002}$	$1.3^{+0.1}_{-0.1}$	13^{+16}_{-6}	22^{+1}_{-1}	24^{+1}_{-1}
A2029	2.2	$0.37^{+0.04}_{-0.03}$	$2.9^{+0.2}_{-0.2}$	54^{+31}_{-3}	< 21	1160^{+9}_{-11}
A2052	5.5	$0.017^{+0.002}_{-0.002}$	$0.71^{+0.04}_{-0.08}$	94^{+125}_{-4}	$8.82^{+0.57}_{-0.85}$	94^{+1}_{-1}
MKW 3S	7.8	$0.028^{+0.006}_{-0.009}$	$2.8^{+0.8}_{-0.5}$	256^{+262}_{-28}	< 0.95	99^{+3}_{-4}
A2199	4.4	$0.099^{+0.005}_{-0.005}$	$2.2^{+0.2}_{-0.1}$	169^{+156}_{-38}	$1.87^{+1.25}_{-1.25}$	142^{+1}_{-3}
Hercules A	67.0	$0.0111^{+0.0006}_{-0.0005}$	$2.0^{+0.2}_{-0.2}$	10000	< 34	210^{+6}_{-52}
3C 388	55.6	$0.0069^{+0.0004}_{-0.0004}$	$3.0^{+0.2}_{-0.2}$	125^{+175}_{-50}	43^{+21}_{-21}	27^{+2}_{-4}
Cygnus A	5.3	$0.132^{+0.009}_{-0.008}$	$5.2^{+0.5}_{-0.6}$	2440	19200^{+451}_{-451}	370^{+11}_{-11}
Sersic 159/03	12.2	$0.056^{+0.004}_{-0.004}$	$1.8^{+0.2}_{-0.1}$	488^{+512}_{-162}	< 0.57	211^{+8}_{-8}
A2597	11.0	$0.073^{+0.005}_{-0.005}$	$1.6^{+0.2}_{-0.2}$	42^{+54}_{-18}	< 23	440^{+20}_{-36}
A4059	10.6	$0.022^{+0.001}_{-0.001}$	$2.1^{+0.1}_{-0.1}$	60^{+56}_{-22}	< 0.44	91^{+1}_{-1}

Table 3. Parameters for the Bondi Accretion

System	r_B (kpc)	$n_{e,B}$ (cm^{-3})	T_B (keV)	\dot{M}_B ($M_\odot \text{ yr}^{-1}$)	P_B ($10^{44} \text{ erg s}^{-1}$)
A85	$0.15^{+0.31}_{-0.10}$	$2.73^{+0.73}_{-0.81}$	$1.56^{+0.17}_{-0.15}$	$0.85^{+5.60}_{-0.75}$	48^{+318}_{-43}
A133	$0.13^{+0.27}_{-0.09}$	$5.68^{+1.92}_{-2.16}$	$0.73^{+0.08}_{-0.06}$	$1.01^{+5.42}_{-0.89}$	58^{+307}_{-51}
A262	$0.029^{+0.063}_{-0.020}$	$0.76^{+0.20}_{-0.15}$	$0.67^{+0.06}_{-0.05}$	$0.006^{+0.052}_{-0.005}$	$0.35^{+2.93}_{-0.31}$
Perseus	$0.013^{+0.028}_{-0.009}$	34^{+13}_{-9}	$0.86^{+0.09}_{-0.08}$	$0.062^{+0.513}_{-0.055}$	$3.5^{+29.1}_{-3.1}$
2A 0335+096	$0.092^{+0.203}_{-0.062}$	$1.27^{+0.97}_{-0.52}$	$1.07^{+0.27}_{-0.24}$	$0.13^{+1.13}_{-0.11}$	$7.2^{+64.0}_{-6.5}$
A478	$0.17^{+0.33}_{-0.11}$	$7.93^{+10.16}_{-4.22}$	$1.12^{+0.29}_{-0.21}$	$2.78^{+17.71}_{-2.48}$	158^{+1000}_{-141}
MS 0735.6+7421	$0.15^{+0.32}_{-0.10}$	74^{+3436}_{-57}	$1.09^{+0.28}_{-0.22}$	$20.07^{+1572.5}_{-18.50}$	1140^{+89100}_{-1050}
PKS 0745-191	$0.17^{+0.35}_{-0.11}$	25^{+70}_{-15}	$1.09^{+0.28}_{-0.22}$	$8.23^{+84.95}_{-7.43}$	466^{+4810}_{-421}
Hydra A	$0.11^{+0.24}_{-0.08}$	11^{+6}_{-5}	$1.69^{+0.19}_{-0.15}$	$2.10^{+12.07}_{-1.86}$	119^{+684}_{-106}
Zw 2701	$0.19^{+0.40}_{-0.13}$	36^{+57}_{-24}	$1.10^{+0.28}_{-0.22}$	$16.53^{+105.51}_{-15.13}$	937^{+5980}_{-858}
Zw 3146	$0.27^{+0.51}_{-0.18}$	$5.72^{+19.59}_{-3.37}$	$1.11^{+0.31}_{-0.20}$	$4.89^{+57.30}_{-4.39}$	277^{+3250}_{-249}
M84	$0.012^{+0.026}_{-0.008}$	$9.86^{+25.29}_{-7.22}$	$1.01^{+0.02}_{-0.02}$	$0.016^{+0.171}_{-0.015}$	$0.88^{+9.67}_{-0.83}$
M87	$0.15^{+0.42}_{-0.11}$	$8.16^{+14.66}_{-7.32}$	$1.36^{+0.06}_{-0.22}$	$2.60^{+3.58}_{-2.34}$	148^{+203}_{-133}
Centaurus	$0.080^{+0.175}_{-0.055}$	$2.19^{+0.38}_{-0.67}$	$0.82^{+0.04}_{-0.04}$	$0.15^{+0.90}_{-0.13}$	$8.3^{+50.9}_{-7.3}$
HCG 62	$0.020^{+0.046}_{-0.014}$	$4.16^{+36.99}_{-3.63}$	$1.06^{+0.27}_{-0.25}$	$0.020^{+0.497}_{-0.019}$	$1.1^{+28.2}_{-1.1}$
A1795	$0.062^{+0.130}_{-0.042}$	$1.17^{+0.23}_{-0.20}$	$1.17^{+0.07}_{-0.06}$	$0.055^{+0.442}_{-0.049}$	$3.1^{+25.0}_{-2.8}$
A1835	$0.20^{+0.41}_{-0.13}$	$7.00^{+8.50}_{-3.90}$	$1.10^{+0.28}_{-0.22}$	$3.36^{+26.44}_{-3.06}$	191^{+1500}_{-173}
PKS 1404-267	$0.027^{+0.057}_{-0.018}$	$9.02^{+3.47}_{-4.06}$	$0.86^{+0.04}_{-0.04}$	$0.068^{+0.489}_{-0.063}$	$3.9^{+27.7}_{-3.5}$
A2029	$0.067^{+0.137}_{-0.045}$	$1.72^{+0.28}_{-0.27}$	$1.97^{+0.12}_{-0.09}$	$0.12^{+0.92}_{-0.11}$	$7.0^{+52.2}_{-6.2}$
A2052	$0.11^{+0.24}_{-0.08}$	$0.53^{+0.47}_{-0.27}$	$0.60^{+0.06}_{-0.06}$	$0.057^{+0.437}_{-0.052}$	$3.2^{+24.8}_{-2.9}$
MKW 3S	$0.061^{+0.130}_{-0.041}$	$1.02^{+1.11}_{-0.52}$	$1.08^{+0.28}_{-0.23}$	$0.045^{+0.403}_{-0.041}$	$2.5^{+22.8}_{-2.3}$
A2199	$0.073^{+0.150}_{-0.049}$	$3.81^{+5.45}_{-1.17}$	$1.22^{+0.07}_{-0.05}$	$0.26^{+2.31}_{-0.22}$	15^{+131}_{-13}
Hercules A	$0.077^{+0.173}_{-0.052}$	$1.28^{+2.01}_{-0.70}$	$1.07^{+0.27}_{-0.25}$	$0.089^{+1.032}_{-0.082}$	$5.1^{+58.5}_{-4.7}$
3C 388	$0.069^{+0.151}_{-0.047}$	$0.65^{+1.23}_{-0.41}$	$2.13^{+0.27}_{-0.26}$	$0.053^{+0.542}_{-0.049}$	$3.0^{+30.7}_{-2.8}$
Cygnus A	$0.078^{+0.151}_{-0.052}$	$3.39^{+1.23}_{-1.07}$	$1.13^{+0.30}_{-0.21}$	$0.25^{+1.58}_{-0.23}$	14^{+90}_{-13}
Sersic 159/03	$0.061^{+0.138}_{-0.042}$	$1.02^{+0.67}_{-0.37}$	$1.07^{+0.27}_{-0.24}$	$0.046^{+0.447}_{-0.041}$	$2.6^{+25.3}_{-2.4}$
A2597	$0.086^{+0.210}_{-0.060}$	13^{+47}_{-9}	$0.57^{+0.33}_{-0.24}$	$0.84^{+17.18}_{-0.80}$	48^{+974}_{-45}
A4059	$0.29^{+0.58}_{-0.20}$	$4.28^{+1.74}_{-2.13}$	$0.98^{+0.11}_{-0.08}$	$4.14^{+15.65}_{-3.57}$	235^{+887}_{-202}